

# A mouse model of endometriosis mimicking the natural spread of invasive endometrium

Mike R. Wilson<sup>1</sup>, Jeanne Holladay<sup>1</sup>, and Ronald L. Chandler<sup>1,2,3,\*</sup>

<sup>1</sup>Department of Obstetrics, Gynecology and Reproductive Biology, College of Human Medicine, Michigan State University, Grand Rapids, MI 49503, USA <sup>2</sup>Center for Epigenetics, Van Andel Research Institute, Grand Rapids, MI 49503, USA <sup>3</sup>Department of Women's Health, Spectrum Health System, Grand Rapids, MI 49341, USA

\*Correspondence address. Grand Rapids Research Center (GRRC), 400 Monroe Ave. NW, Room 3009, Grand Rapids, Michigan, United States, 49503; E-mail: rlc@msu.edu

Submitted on August 16, 2019; resubmitted on September 27, 2019; editorial decision on October 23, 2019

**STUDY QUESTION:** Is it possible to establish a genetically engineered mouse model (GEMM) of endometriosis that mimics the natural spread of invasive endometrium?

**SUMMARY ANSWER:** Endometriosis occurs in an ARID1A (AT-rich interactive domain-containing protein 1A) and PIK3CA (phosphatidylinositol-4,5-bisphosphate 3-kinase, catalytic subunit alpha) mutant GEMM of endometrial dysfunction following salpingectomy.

**WHAT IS KNOWN ALREADY:** Although mouse models of endometriosis have long been established, most models rely on intraperitoneal injection of uterine fragments, steroid hormone treatments or the use of immune-compromised mice.

**STUDY DESIGN, SIZE, DURATION:** Mice harboring the lactotransferrin-Cre (*LtfCre*<sup>0/+</sup>), *Arid1a*<sup>fl</sup>, (*Gt*)*R26Pik3ca*<sup>\*H1047R</sup> and (*Gt*)*R26<sup>mTmG</sup>* alleles were subject to unilateral salpingectomies at 6 weeks of age. Control (*n* = 9), *LtfCre*<sup>0/+</sup>; (*Gt*)*R26Pik3ca*<sup>\*H1047R</sup>; *Arid1a*<sup>fl/+</sup> (*n* = 8) and *LtfCre*<sup>0/+</sup>; (*Gt*)*R26Pik3ca*<sup>\*H1047R</sup>; *Arid1a*<sup>fl/fl</sup> (*n* = 9) were used for the study. The (*Gt*)*R26<sup>mTmG</sup>* allele was used for the purpose of fluorescent lineage tracing of endometrial epithelium. *LtfCre*<sup>0/+</sup>; (*Gt*)*R26<sup>mTmG</sup>* (*n* = 3) and *LtfCre*<sup>0/+</sup>; (*Gt*)*R26Pik3ca*<sup>\*H1047R/mTmG</sup>; *Arid1a*<sup>fl/fl</sup> (*n* = 4) were used for this purpose. Mice were followed until the endpoint of vaginal bleeding at an average time of 17 weeks of age.

**PARTICIPANTS/MATERIALS, SETTING, METHODS:** At 6 weeks of age, mice were subjected to salpingectomy surgery. Mice were followed until the time point of vaginal bleeding (average 17 weeks), or aged for 1 year in the case of control mice. At time of sacrifice, endometriotic lesions, ovaries and uterus were collected for the purpose of histochemical and immunohistochemical analyses. Samples were analyzed for markers of the endometriotic tissue and other relevant biomarkers.

**MAIN RESULTS AND THE ROLE OF CHANCE:** Following salpingectomy, *LtfCre*<sup>0/+</sup>; (*Gt*)*R26Pik3ca*<sup>\*H1047R/mTmG</sup>; *Arid1a*<sup>fl/fl</sup> mice developed endometriotic lesions, including lesions on the ovary, omentum and abdominal wall. Epithelial glands within lesions were negative for ARID1A and positive for phospho-S6 staining, indicating ARID1A-PIK3CA co-mutation status, and expressed EGFP (enhanced green fluorescent protein), indicating endometrial origins.

**LARGE-SCALE DATA:** N/A

**LIMITATIONS, REASONS FOR CAUTION:** *LtfCre*<sup>0/+</sup>; (*Gt*)*R26Pik3ca*<sup>\*H1047R</sup>; *Arid1a*<sup>fl/fl</sup> mice develop vaginal bleeding as a result of endometrial dysfunction at an average age of 17 weeks and must be sacrificed. Furthermore, while this model mimics the natural spread of endometriotic tissue directly from the uterus to the peritoneum, the data presented do not reject current hypotheses on endometriosis pathogenesis.

**WIDER IMPLICATIONS OF THE FINDINGS:** The idea that endometriosis is the result of abnormal endometrial tissue colonizing the peritoneum via retrograde menstruation has gained widespread support over the past century. However, most models of endometriosis take for granted this possibility, relying on the surgical removal of bulk uterine tissue and subsequent transplantation into the peritoneum. Growing evidence suggests that somatic mutations in ARID1A and PIK3CA are present in the endometrial epithelium. The establishment of a GEMM which mimics the natural spread of endometrium and subsequent lesion formation supports the hypothesis that endometriosis is derived from mutant endometrial epithelium with invasive properties.

**STUDY FUNDING/COMPETING INTEREST(S):** This research was supported by the American Cancer Society PF-17-163-02-DDC (M.R.W.), the Mary Kay Foundation 026-16 (R.L.C.) and the Ovarian Cancer Research Fund Alliance 457446 (R.L.C.). The authors declare no competing interests.

**Key words:** endometriosis / mouse / invasion / endometrium / uterus

## Introduction

Endometriosis is a disease in which cells lining the uterus (endometrium) grow outside of the uterus, causing pain and infertility in 5 to 10% of women (Alimi et al., 2018). Formation of endometriosis is thought to result from the translocation of endometrium via retrograde menstruation (Chui et al., 2017). The retrograde menstruation theory is supported by several clinical observations that obstruction of menstrual flow increases the incidence of endometriosis (Burney and Giudice, 2012). Other theories for endometriosis pathogenesis propose that lesions arise from peritoneal tissue or extra-uterine stem cells which have become transformed into ectopic endometrium, while additional theories hold that endometrium arrives into the peritoneum by lymphatic or hematogenous dissemination (Burney and Giudice, 2012). Studies have suggested that the invasive phenotype of endometriosis shares aspects with tumor metastasis, including migration and invasion (Giudice and Kao, 2004). In order for endometriosis to occur, endometrial cells may undergo epithelial-to-mesenchymal transition (EMT) in order to invade distal tissues (Bartley et al., 2014), a probable scenario given the inherent plasticity of the endometrium (Matsuzaki and Darcha, 2012).

Mutations in ARID1A (AT-rich interactive domain-containing protein 1A), a well-established tumor suppressor gene, are also found in endometriosis (Samartzis et al., 2012), and ARID1A loss may indicate malignancy in atypical endometriosis (Wiegand et al., 2011). Additionally, mutations in PIK3CA (phosphatidylinositol-4,5-bisphosphate 3-kinase, catalytic subunit alpha) may be a prerequisite to ARID1A loss in endometriosis (Anglesio et al., 2017; Suda et al., 2018).

Recently, we characterized a new genetically engineered mouse model of endometrial dysfunction which results in endometrial hyperplasia, vaginal bleeding and lesion formation (Wilson et al., 2019). We utilized the lactotransferrin-Cre (*LtfCre*) allele, which drives Cre-recombinase expression specifically to the endometrial epithelium. The mice displayed loss of ARID1A expression and expression of the oncogenic PIK3CA<sup>H1047R</sup> mutation, resulting in endometrial hyperplasia, lesion formation and invasion into the uterine myometrium (Wilson et al., 2019). We employed genome-wide methodologies to examine changes in gene expression and chromatin accessibility of sorted endometrial epithelial cells *in vivo* and identified upregulation of EMT pathways and epithelial transdifferentiation in the mutant cells. We found that ARID1A and PIK3CA mutant endometrial epithelium was capable of invasion locally into the myometrium (Wilson et al., 2019). Given that endometriosis may be derived from invasive endometrial epithelium and ARID1A and PIK3CA mutations, we sought to utilize our model of endometrial dysfunction to explore the development of endometriosis.

Mice do not menstruate; therefore, the opportunity for endometrial tissue to translocate to the peritoneum via retrograde menstruation does not exist in mice. Traditional mouse models of endometriosis were developed via the surgical transplantation of autologous or

syngeneic uterine tissue into the peritoneum (Cummings and Metcalf, 1995; Hirata et al., 2005; Rossi et al., 2000; Cheng et al., 2011; Greaves et al., 2014), or transplantation of human endometrial or endometriotic tissue into immune-compromised mice (Aoki et al., 1994; Grummer et al., 2001), often with estrogen supplementation (Zamah et al., 1984; Bergqvist et al., 1985). Previously developed genetically engineered mouse models of endometriosis have relied on mutation of genes in the ovarian surface epithelium rather than the endometrium (Dinulescu et al., 2005; Budiu et al., 2009). Here, we developed a model of endometriosis derived from the endometrial epithelium by surgical incision at the uterotubal junction followed by salpingectomy in mice harboring ARID1A and PIK3CA mutations in the endometrial epithelium. This procedure created an opening in the uterus at the uterotubal junction, thereby exposing the uterine cavity and providing mutant cells an opening to invade into the peritoneal cavity, resulting in endometriosis formation. In this study, we have characterized a new genetically engineered mouse model of endometriosis derived from mutant endometrial epithelium which mimics the natural spread of invasive endometrium.

## Materials and Methods

### Contact for reagent and resource sharing

Requests for further information, resources and reagents should be addressed to the lead contact, Ronald L. Chandler (rlc@msu.edu).

### Mice

All mice were maintained on an outbred genetic background using CD-1 mice (Charles River, Wilmington, MA, USA). (*Gt*)R26<sup>mTmG</sup>, (*Gt*)R26Pik3ca<sup>\*H1047R</sup> and *LtfCre* (*Tg(Ltf:Cre)14Mmul*) alleles were purchased from The Jackson Laboratory (Bar Harbor, ME, USA) and identified by PCR using published methods (Muzumdar et al., 2007; Adams et al., 2011; Daikoku et al., 2014). The *Arid1a*<sup>fl</sup> allele was detected by PCR as previously described (Chandler et al., 2013; Chandler et al., 2015). Endpoints were vaginal bleeding, severe abdominal distension and signs of severe illness, such as dehydration, hunching, jaundice, ruffled fur, signs of infection or non-responsiveness. Sample sizes within each genotype were chosen based on the proportions of animals with vaginal bleeding between each experimental group or a Kaplan–Meyer log-rank test for survival differences. Mice were housed at the Van Andel Research Institute Animal Facility and the Michigan State University Grand Rapids Research Center in accordance with protocols approved by Michigan State University. Michigan State University is registered with the US Department of Agriculture (USDA) and has an approved Animal Welfare Assurance from the NIH Office of Laboratory Animal Welfare (OLAW). MSU is accredited by the Association for Assessment and Accreditation of Laboratory Animal Care (AAALAC).

**Table I Immunohistochemistry antibodies.**

Antibody	Dilution	Source	Identifier
Rabbit monoclonal anti-ARID1A/BAF250A (D2A8U)	1:200	Cell Signaling Technology	Cat# 12354; RRID: AB_2637010
Rabbit monoclonal anti-Phospho-S6 Ribosomal Protein (Ser235/236) (D57.2.2E)	1:400	Cell Signaling Technology	Cat# 4858; RRID: AB_2721245
Rat monoclonal anti-TROMA-I	1:100	Developmental Studies Hybridoma Bank	Cat# TROMA-I; RRID: AB_531826
Goat polyclonal anti-ICAM-1/CD54	1:100	R&D Systems	Cat# AF796-SP; RRID: AB_2248703
Rat monoclonal anti-FRA-2 (REY146C)	1:200	EMD Millipore	Cat# MABS1261
Rabbit monoclonal anti-c-Jun (60A8)	1:300	Cell Signaling Technology	Cat# 9165; RRID: AB_2130165
Rabbit monoclonal anti-Ki67 (D3B5)	1:400	Cell Signaling Technology	Cat# 12202; RRID: AB_2620142

RRID, Research Resource Identifier; ARID1A, AT-rich interactive domain-containing protein 1A; ICAM-1, intercellular adhesion molecule 1; Fra2, Fos-related antigen 2; TROMA-I, trophectoderm-specific marker 1.

## Uterotubal incision and salpingectomy surgery

Ovarian surgical protocol was followed as previously described (Chandler *et al.*, 2015). Mice were anaesthetized using avertin (0.3 mg/g intraperitoneal injection). Avertin was composed of sterile embryo water (Sigma, cat# W1503, St. Louis, MO, USA), 2-methyl-2-butanol (Sigma, cat# 152463) and 2,2,2-tribromoethanol (Sigma, cat# T48402). Anesthesia was confirmed by the absence of reflex withdrawal to toe pinch. Hair at the procedure site was removed with small electric shears and scrubbed with betadine solution (Povidone-Iodine Veterinary Surgical Scrub, McKesson, Pompano Beach, FL, USA). Salpingectomy surgeries were performed on 6-week-old mice. Following incision through the left flank muscle, the ovary was removed and an incision was made at the uterotubal junction, being careful to avoid the uterine artery. Following uterotubal incision, the oviduct was removed. During the procedure, the ovary was kept moistened using a gauze soaked in PBS. The ovary was gently placed back, and the muscle layer was closed using sutures. Following surgery, mice were monitored for basic biologic functions and post-procedure distress. Surgeries were performed in the afternoon. The surgeon was blinded from the genotype of the mouse. Mice were housed randomly following surgery. All surgical data has been reported to ensure the study is free of selective outcome reporting.

## Histology and immunohistochemistry

Upon vaginal bleeding, mice were euthanized by carbon dioxide inhalation and uterus, ovaries and relevant tissues were collected. For indirect immunohistochemistry (IHC), 10% neutral buffered formalin (NBF)-fixed paraffin sections were processed for heat-based antigen unmasking in 10 mM sodium citrate (pH 6.0). Sections were incubated with antibodies at the following dilutions: 1:200 ARID1A (12354, Cell Signaling, Danvers, MA); 1:400 Phospho-S6 (4585, Cell Signaling); 1:100 KRT8 (Ketatin 8) (TROMA1, DSHB); 1:100 ICAM-1 (intercellular adhesion molecule 1) (AF796-SP, R&D Systems, Minneapolis, MN, USA); 1:200 Fra2 (MABS1261, EMD Millipore, Burlington, MA, USA); 1:300 c-Jun (9165, Cell Signaling); and 1:400 Ki67 (12202, Cell Signaling). TROMA-I antibody was deposited to the Developmental Studies Hybridoma Bank (DSHB) by Brulet, P./Kemler, R. (DSHB Hybridoma Product TROMA-I). Primary antibody dilutions and catalog numbers are compiled in Table I. The following biotin-conjugated

secondary antibodies were used: donkey anti-rabbit IgG (711-065-152, Jackson ImmunoResearch Lab, West Grove, PA, USA) and donkey anti-rat IgG (#705-065-153, Jackson ImmunoResearch Lab). Secondary antibodies were detected using VECTASTAIN Elite ABC HRP Kit (Vector, Burlingame, CA, USA). Sections for IHC were lightly counterstained with Hematoxylin QS or Methyl Green (Vector Labs). Routine hematoxylin and eosin (H&E) staining of sections was performed by the Van Andel Research Institute (VARI) Histology and Pathology Core. A VARI animal pathologist reviewed histological sections. For picosirius red staining, the Picosirius Red Stain Kit (Polysciences, Inc., Warrington, PA, USA, cat# 24901-250) was used according to the manufacturers' instructions.

## Microscopy and imaging

Fluorescent images were taken using a Nikon SMZ18 microscope, X-Cite Series 120 PC Q (Excelitas Technologies, Waltham, MA, USA) fluorescent lamp and a Nikon DS-Ri1 camera. Images were analyzed using Nikon NIS Elements Advanced Research software.

## Statistics

Statistical analyses were performed using GraphPad (San Diego, CA, USA) Prism 8 software.

## Results

### Salpingectomy of genetically engineered mice results in a broad spectrum of endometriotic phenotypes

To determine if the invasive cellular phenotypes observed in *LtfCre*<sup>0/+</sup>; (*Gt*)*R26Pik3ca*<sup>\*H1047R</sup>; *Arid1a*<sup>fl/+</sup> and *LtfCre*<sup>0/+</sup>; (*Gt*)*R26Pik3ca*<sup>\*H1047R</sup>; *Arid1a*<sup>fl/fl</sup> mice (Fig. 1A) promote the extrauterine spread of mutant endometrial epithelium, we devised a surgical protocol that mimics retrograde translocation of endometrial tissue into the peritoneal space (Fig. 1B and C). In contrast to humans, the isthmus and ampulla of mouse oviducts are tightly coiled and the infundibulum of the mouse oviduct opens into the bursal space, rather than the peritoneal cavity (Rendi *et al.*, 2012). We reasoned that exposing the endometrial lumen and removing the anatomic barrier of the oviducts and bursal membrane via surgery would allow invasive luminal endometrial

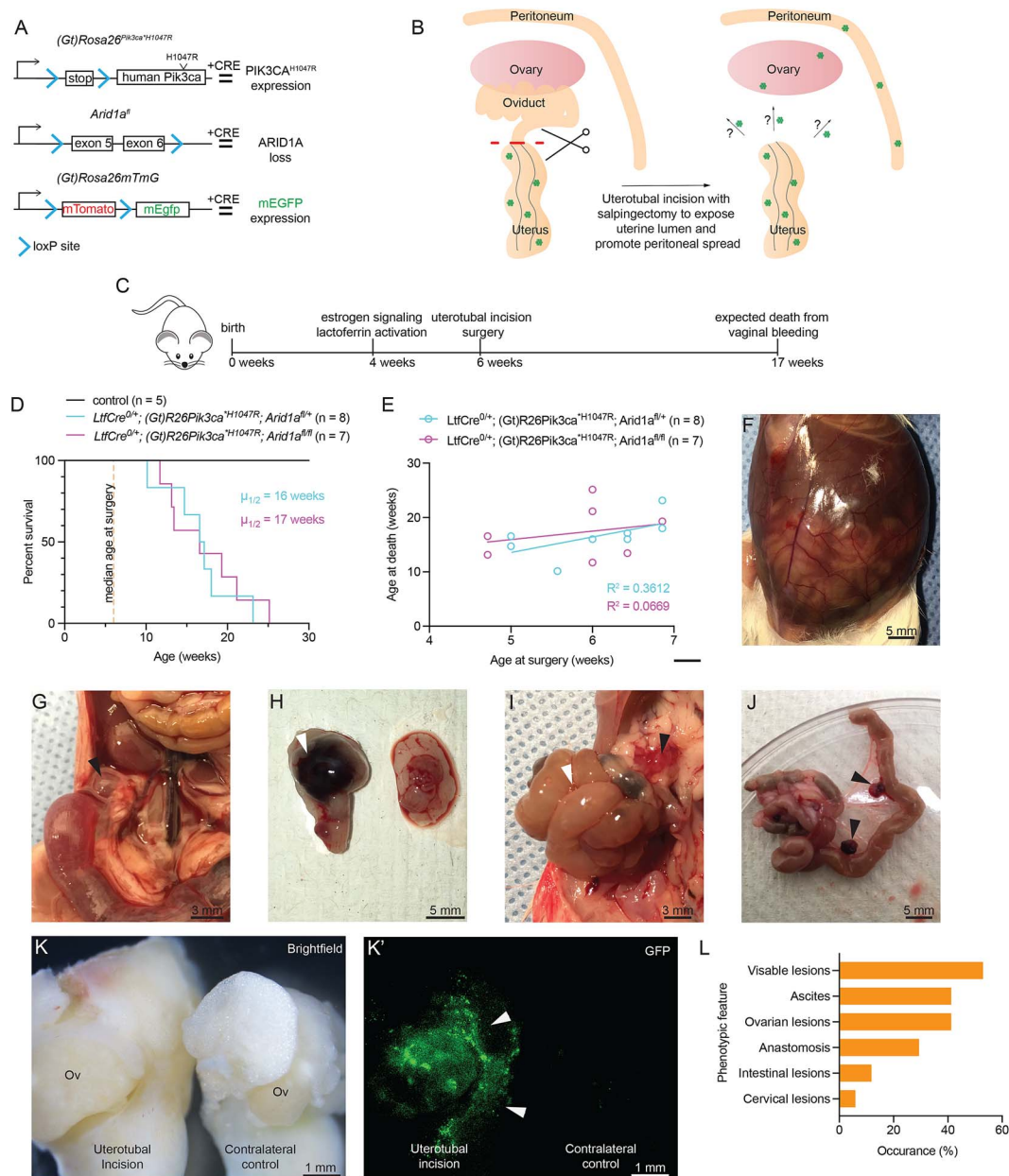


**Figure 1** *LtfCre*<sup>0/+</sup>; (Gt)R26Pik3ca<sup>\*H1047R</sup>; *Arid1a*<sup>fl/fl</sup> and *LtfCre*<sup>0/+</sup>; (Gt)R26Pik3ca<sup>\*H1047R</sup>; *Arid1a*<sup>fl/fl</sup> mice develop ovarian lesions, anastomosis and ascites following salpingectomy. (A) Diagram depicting mouse alleles used in this study. ARID1A, AT-rich interactive domain-containing protein 1A; PIK3CA, phosphatidylinositol-4,5-bisphosphate 3-kinase, catalytic subunit alpha; mEGFP, mouse enhanced green fluorescent protein. (B) Schematic representation of uterotubal incision and salpingectomy surgery. (C) Timeline for experimental mouse model. (D) Survival of mice following surgery. Survival was based on vaginal bleeding and other endpoints (see Table II). Control mice were aged for 1 year (*n* = 9, black line). No difference in survival was observed between *LtfCre*<sup>0/+</sup>; (Gt)R26Pik3ca<sup>\*H1047R</sup>; *Arid1a*<sup>fl/fl</sup> (*n* = 8, blue line) and *LtfCre*<sup>0/+</sup>; (Gt)R26Pik3ca<sup>\*H1047R</sup>; *Arid1a*<sup>fl/fl</sup> (*n* = 9, purple line) mice following surgery (*P* = 0.7421, unpaired *t* test, two-tailed). (E) Age at surgery vs. age at death. No significant relationship was observed (*P* = 0.1151 for *LtfCre*<sup>0/+</sup>; (Gt)R26Pik3ca<sup>\*H1047R</sup>; *Arid1a*<sup>fl/fl</sup>, blue line; *P* = 0.3584 for *LtfCre*<sup>0/+</sup>; (Gt)R26Pik3ca<sup>\*H1047R</sup>; *Arid1a*<sup>fl/fl</sup>, purple line Pearson's). (F) Example of *LtfCre*<sup>0/+</sup>; (Gt)R26Pik3ca<sup>\*H1047R</sup>; *Arid1a*<sup>fl/fl</sup> mice with ascites following surgery. (G) Ovarian cysts are observed in animals 6 weeks post-salpingectomy on the ipsilateral ovary. Arrow indicates cyst. (H) Example of animal with hemorrhagic 'chocolate cyst' endometrioma on ovary ipsilateral to incision. Arrow indicates lesion. (I) Intestinal obstruction in mutant mice following surgery. White arrows denote intestines, black arrows denote omental metastasis. (J) Intestinal anastomosis following salpingectomy. Black arrows denote omental lesions. (K) Bright-field image and fluorescent green image (K'). EGFP fluorescence denotes Cre + endometrial epithelium on or near the ovary. Ov: ovary. (L) Histogram compiling observational data upon necropsy.

**Table II** Summary of mice.

Genotype	Age at surgery (days)	Age at death (days)	Cause of death/ reason for sacrifice	Observations
Control	42	43	FD	Complications from surgery
Control	35	103	ED	No phenotype
Control	35	103	ED	No phenotype
Control	35	103	ED	No phenotype
Control	42	403	ES	No phenotype
Control	45	406	ES	No phenotype
Control	45	406	ES	No phenotype
Control	45	406	ES	No phenotype
Control	48	418	ES	No phenotype
<i>LtfCre</i> <sup>0/+</sup> ; <i>Arid1a</i> <sup>fl/+</sup> ; ( <i>Gt</i> ) <i>R26Pik3ca</i> <sup>*H1047R</sup>	39	71	VB	
<i>LtfCre</i> <sup>0/+</sup> ; <i>Arid1a</i> <sup>fl/+</sup> ; ( <i>Gt</i> ) <i>R26Pik3ca</i> <sup>*H1047R</sup>	35	103	VB	Lesion on ipsilateral ovary
<i>LtfCre</i> <sup>0/+</sup> ; <i>Arid1a</i> <sup>fl/+</sup> ; ( <i>Gt</i> ) <i>R26Pik3ca</i> <sup>*H1047R</sup>	42	112	AB, VB	Lesions throughout peritoneum, organ anastomosis, ascites
<i>LtfCre</i> <sup>0/+</sup> ; <i>Arid1a</i> <sup>fl/+</sup> ; ( <i>Gt</i> ) <i>R26Pik3ca</i> <sup>*H1047R</sup>	45	112	FD	
<i>LtfCre</i> <sup>0/+</sup> ; <i>Arid1a</i> <sup>fl/+</sup> ; ( <i>Gt</i> ) <i>R26Pik3ca</i> <sup>*H1047R</sup>	35	116	VB	Intestinal anastomosis, ascites
<i>LtfCre</i> <sup>0/+</sup> ; <i>Arid1a</i> <sup>fl/+</sup> ; ( <i>Gt</i> ) <i>R26Pik3ca</i> <sup>*H1047R</sup>	45	120	VB, DA	Ovarian lesions, intestinal anastomosis, ascites
<i>LtfCre</i> <sup>0/+</sup> ; <i>Arid1a</i> <sup>fl/+</sup> ; ( <i>Gt</i> ) <i>R26Pik3ca</i> <sup>*H1047R</sup>	48	126	Distressed, VB	Lesions on both ovaries and omentum, intestinal anastomosis
<i>LtfCre</i> <sup>0/+</sup> ; <i>Arid1a</i> <sup>fl/+</sup> ; ( <i>Gt</i> ) <i>R26Pik3ca</i> <sup>*H1047R</sup>	48	162	VB, DA	Ascites
<i>LtfCre</i> <sup>0/+</sup> ; <i>Arid1a</i> <sup>fl/fl</sup> ; ( <i>Gt</i> ) <i>R26Pik3ca</i> <sup>*H1047R</sup>	42	82	Lethargic, pale	Lesion on cervix, blood in intestines
<i>LtfCre</i> <sup>0/+</sup> ; <i>Arid1a</i> <sup>fl/fl</sup> ; ( <i>Gt</i> ) <i>R26Pik3ca</i> <sup>*H1047R</sup>	33	92	VB	
<i>LtfCre</i> <sup>0/+</sup> ; <i>Arid1a</i> <sup>fl/fl</sup> ; ( <i>Gt</i> ) <i>R26Pik3ca</i> <sup>*H1047R</sup>	45	94	DA	Lesions on ovary and mesentery
<i>LtfCre</i> <sup>0/+</sup> ; <i>Arid1a</i> <sup>fl/fl</sup> ; ( <i>Gt</i> ) <i>R26Pik3ca</i> <sup>*H1047R</sup>	48	98	ED	Lesion on ovary
<i>LtfCre</i> <sup>0/+</sup> ; <i>Arid1a</i> <sup>fl/fl</sup> ; ( <i>Gt</i> ) <i>R26Pik3ca</i> <sup>*H1047R</sup>	48	98	ED	Intestinal anastomosis, ascites
<i>LtfCre</i> <sup>0/+</sup> ; <i>Arid1a</i> <sup>fl/fl</sup> ; ( <i>Gt</i> ) <i>R26Pik3ca</i> <sup>*H1047R</sup>	33	116	VB	Intestinal anastomosis, ascites
<i>LtfCre</i> <sup>0/+</sup> ; <i>Arid1a</i> <sup>fl/fl</sup> ; ( <i>Gt</i> ) <i>R26Pik3ca</i> <sup>*H1047R</sup>	48	135	Distressed, VB	Anemic intestines
<i>LtfCre</i> <sup>0/+</sup> ; <i>Arid1a</i> <sup>fl/fl</sup> ; ( <i>Gt</i> ) <i>R26Pik3ca</i> <sup>*H1047R</sup>	42	148	AB, VB	Ipsilateral ovary fused with kidney, ascites
<i>LtfCre</i> <sup>0/+</sup> ; <i>Arid1a</i> <sup>fl/fl</sup> ; ( <i>Gt</i> ) <i>R26Pik3ca</i> <sup>*H1047R</sup>	42	176	VB	Lesion on ovary
<i>LtfCre</i> <sup>0/+</sup> ; ( <i>Gt</i> ) <i>R26</i> <sup>mTmG</sup>	54	149	ED	No phenotype
<i>LtfCre</i> <sup>0/+</sup> ; ( <i>Gt</i> ) <i>R26</i> <sup>mTmG</sup>	33	94	ED	No phenotype
<i>LtfCre</i> <sup>0/+</sup> ; ( <i>Gt</i> ) <i>R26</i> <sup>mTmG</sup>	64	125	ED	No phenotype
<i>LtfCre</i> <sup>0/+</sup> ; <i>Arid1a</i> <sup>fl/fl</sup> ; ( <i>Gt</i> ) <i>R26Pik3ca</i> <sup>*H1047R/mTmG</sup>	28	123	VB	Lesion on omentum, abdominal wall
<i>LtfCre</i> <sup>0/+</sup> ; <i>Arid1a</i> <sup>fl/fl</sup> ; ( <i>Gt</i> ) <i>R26Pik3ca</i> <sup>*H1047R/mTmG</sup>	38	99	VB	Lesion on ovary
<i>LtfCre</i> <sup>0/+</sup> ; <i>Arid1a</i> <sup>fl/fl</sup> ; ( <i>Gt</i> ) <i>R26Pik3ca</i> <sup>*H1047R/mTmG</sup>	33	92	VB	Lesion on abdominal wall
<i>LtfCre</i> <sup>0/+</sup> ; <i>Arid1a</i> <sup>fl/fl</sup> ; ( <i>Gt</i> ) <i>R26Pik3ca</i> <sup>*H1047R/mTmG</sup>	33	116	VB	Lesion on omentum

Summary of mice. VB, vaginal bleeding; AB, abdominal bulge; FD, found dead; DA, distended abdomen; ES, end of study; ED, explorative dissection.

epithelial cells undergoing delamination and luminal shedding to more easily translocate into the peritoneal space. By performing unilateral salpingectomies at 6 weeks of age, we maximized the period between lactoferrin activation (beginning at 4 weeks) and expected mortality due to vaginal bleeding at 14–17 weeks (Fig. 1C).

Following surgery, mice were followed until vaginal bleeding or other endpoints (Table II). One control mouse died from complication from surgery the following day and was excluded from survival

analysis (Table II). No phenotypes were observed in control mice subjected to salpingectomy and aged for approximately 1 year (Fig. 1D, Table II). *LtfCre*<sup>0/+</sup>; (*Gt*)*R26Pik3ca*<sup>\*H1047R</sup>; *Arid1a*<sup>fl/+</sup> and *LtfCre*<sup>0/+</sup>; (*Gt*)*R26Pik3ca*<sup>\*H1047R</sup>; *Arid1a*<sup>fl/fl</sup> mice lived for an average of 17 weeks, 11 weeks beyond surgery (Fig. 1D). Survival differences between groups following surgery was not significant ( $P = 0.7421$ , unpaired *t* test, two-tailed), and age at time of surgery did not correlate with age at death (Fig. 1E) ( $R^2 = 0.3612$  for *LtfCre*<sup>0/+</sup>; (*Gt*)*R26Pik3ca*<sup>\*H1047R</sup>;

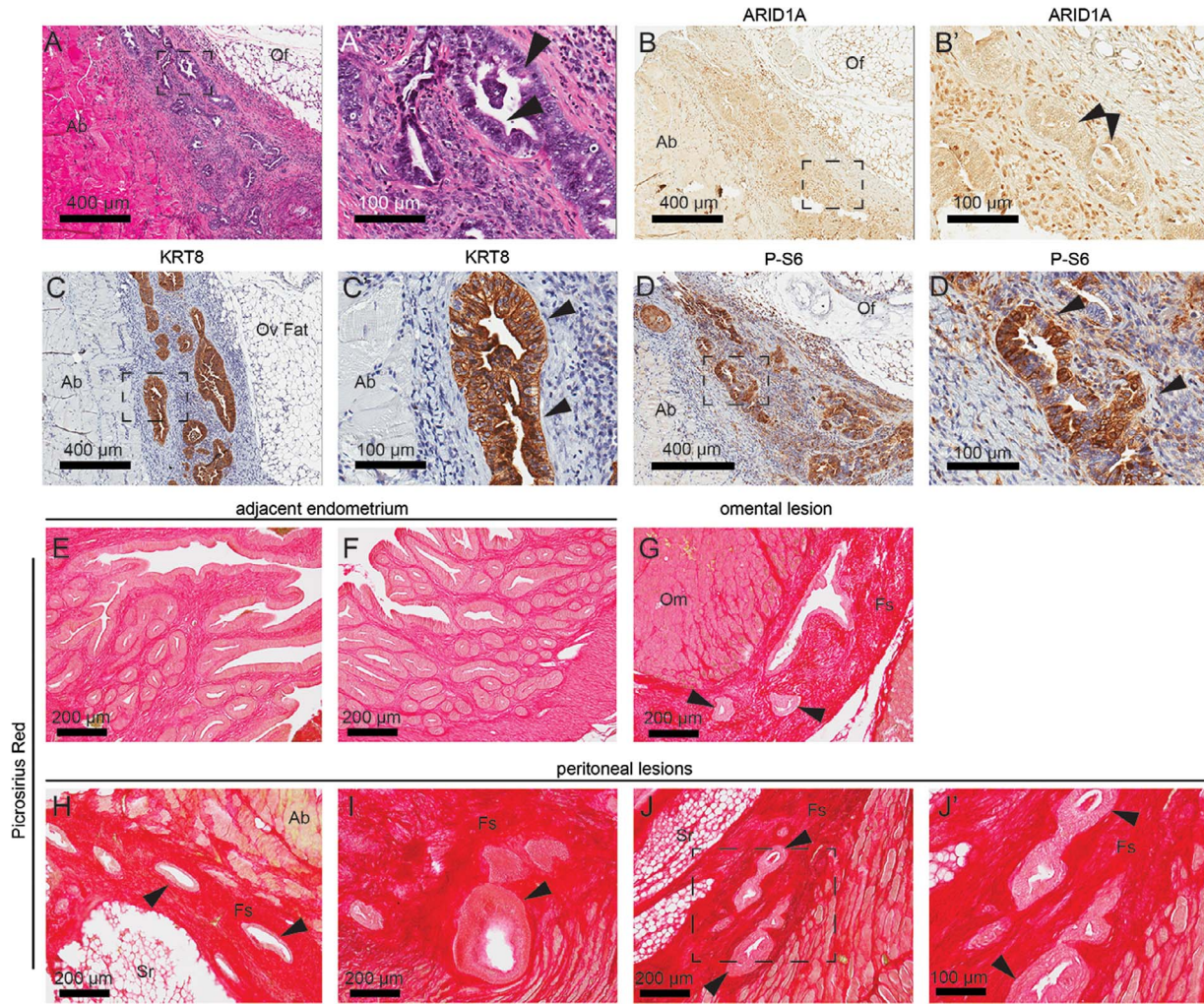


**Figure 2 Endometrial glands formed in ovary are ARID1A-negative.** (A) H&E staining in sections of ovarian lesion. (B–D) Immunohistochemistry (IHC) for ARID1A (B), KRT8 (ketatin 8) (C) and phospho-S6 (P-S6) (D) in sections of ovarian lesion. Panels A–D represent near-adjacent sections of extrauterine endometrial lesions, while panels A'–D' represent portion of slide in panels A–D surrounded by black box. Arrows indicate epithelial gland formation. (E–J) Picrosirius red staining in sections of adjacent uterine tissue (E, F), omental lesions (G) and peritoneal lesions (H–J). Panel J' represents portion in panel J surrounded by black box. Ab: abdominal wall; Cy: cyst; Fs: fibrotic stroma; Of: ovarian fat; Om: omentum; Ov: oocyte; Ov: ovary; Sr: serosa.

*Arid1a*<sup>fl/+</sup>,  $R^2 = 0.0669$  for *LtfCre*<sup>0/+</sup>; (*Gt*)*R26Pik3ca*<sup>\*H1047R</sup>; *Arid1a*<sup>fl/fl</sup>, Pearson's). Following salpingectomy, *LtfCre*<sup>0/+</sup>; (*Gt*)*R26Pik3ca*<sup>\*H1047R</sup>; *Arid1a*<sup>fl/fl</sup> mice developed hemorrhagic ascites within 6 weeks following surgery (Fig. 1F). Extrauterine endometriotic lesions were observed on the ovary (Fig. 1G), with some lesions bearing resemblance to hemorrhagic 'chocolate cyst' endometriomas (Fig. 1H). In some cases, we observed intestinal anastomosis resulting from endometrial spread and fibrosis in the omentum (Fig. 1I and J). *LtfCre* contains an internal ribosomal entry site (IRES)-enhanced green fluorescent protein (EGFP) cassette. Based on EGFP expression, we detected mutant endometrial epithelial cells at sites ipsilateral to the site of incision, but not contralateral ovaries or uterine horns (Fig. 1K). Mice developed a spectrum of phenotypic conditions, including ascites, anastomosis and lesion formation (Fig. 1L). Over 50% of mice displayed visible lesion formation upon dissection (Fig. 1L). The phenotypes observed in this

model reflect the broad spectrum of conditions affecting women with endometriosis.

### Endometrial glands within lesions display markers of ARID1A/PIK3CA mutant endometrium

In order to determine the role of the mutant endometrium in the formation of endometriotic lesions, we used histological analysis and IHC to identify ARID1A and PIK3CA mutant endometrium within lesions. Extrauterine lesions in the ovary were composed of disorganized and dysplastic ARID1A-negative glandular epithelial cells and were observed invading abdominal smooth muscle (Fig. 2A and B). Loss of ARID1A immunoreactivity in the epithelial compartment of the lesions supports endometrial epithelial origins. The extrauterine endometriotic cells also expressed KRT8, a marker of endometrial epithelium,

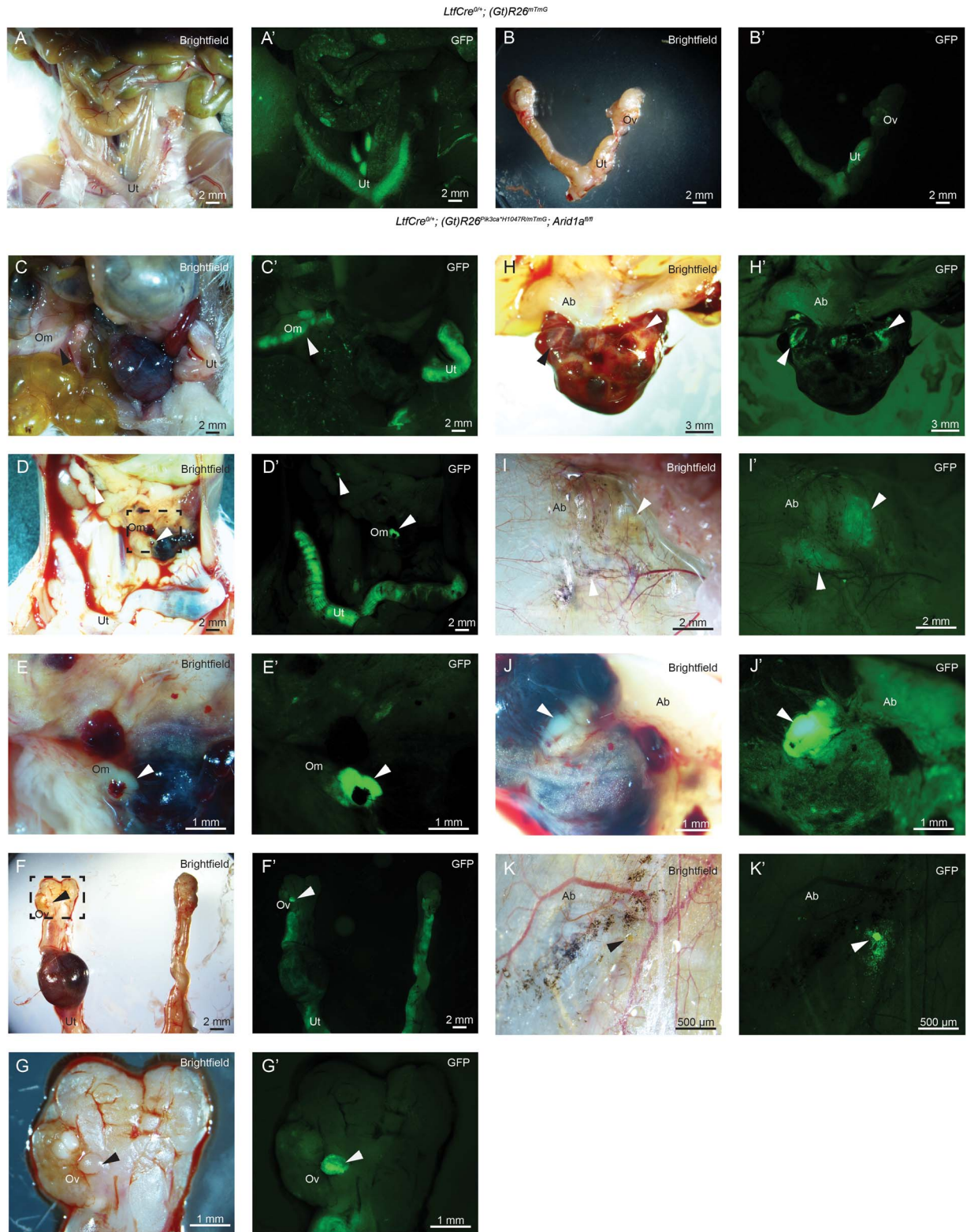


**Figure 3** Lineage tracing of ectopic endometrium with (Gt)R26mTmG allele. (A–K) Bright-field images of mouse intestines and gynecologic tract following salpingectomy. (A'–K') Fluorescent images of the same tissues, depicting cells derived from *Lf1Cre<sup>0/+</sup>; (Gt)R26<sup>mTmG</sup>* ( $n = 3$ ) or *Lf1Cre<sup>0/+</sup>; (Gt)R26<sup>Pik3ca<sup>\*H1047R</sup>/mTmG</sup>; Arid1a<sup>fl/fl</sup>* ( $n = 4$ ) mice. In control mice, GFP expression was confined to the uterus (A–B). In *Lf1Cre<sup>0/+</sup>; (Gt)R26<sup>Pik3ca<sup>\*H1047R</sup>/mTmG</sup>; Arid1a<sup>fl/fl</sup>* mice, lesions were observed on the omentum (C–E), the ovary (F–G) and the peritoneum (H–K). Ab: abdominal wall; Om: omentum; Ov: ovary; Ut: uterus.



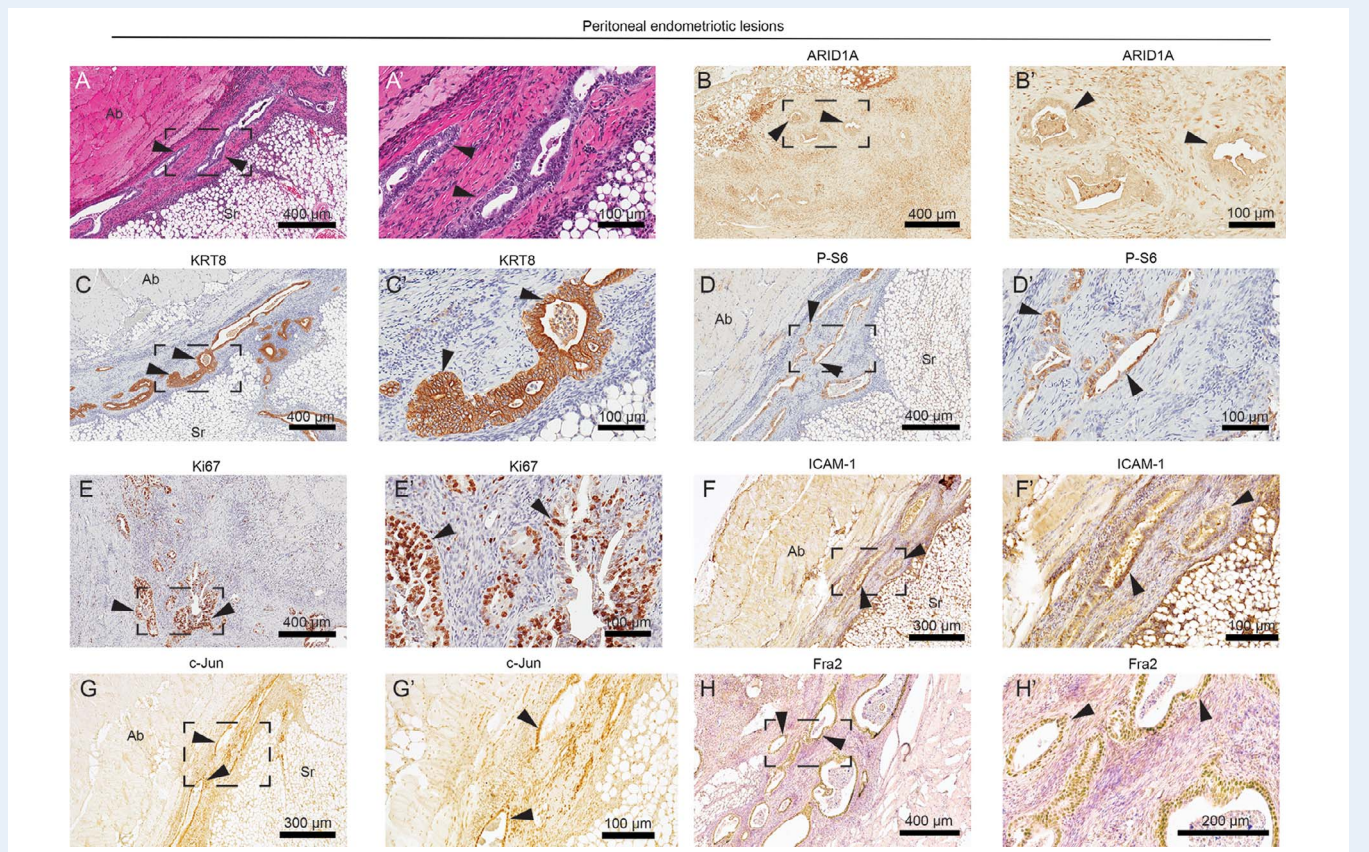


**Figure 5 Biomarker identification in peritoneal endometriotic lesions.** (A) H&E staining of endometrial glands identified in the peritoneum. Endometriotic lesions were fused to the abdominal wall. (B–H) Immunohistochemical staining of peritoneal lesions for ARID1A (B), KRT8 (C), P-S6 (D), Ki67 (E), ICAM-1 (intercellular adhesion molecule 1) (F) and AP-1 (activator protein 1) subunits c-Jun (G) and Fra2 (Fos-related antigen 2) (H). Panels A–H represent near-adjacent sections of peritoneal endometriotic lesions, while panels A'–H' represent portion of slide in panels A–H surrounded by black box. Arrows indicate endometrial glands. Ab: abdominal wall; Sr: serosa.

*LtfCre<sup>0/+</sup>; (Gt)R26Pik3ca<sup>\*H1047R</sup>; Arid1a<sup>fl/fl</sup>* endometrium, which resulted in myometrial invasion and adenomyosis locally within the uterus. Here, we detail a new model of endometriotic spread based on our GEMM of endometrial dysfunction. ARID1A has previously been implicated as a repressor of invasion (Yan *et al.*, 2014; Lakshminarasimhan *et al.*, 2017; Li *et al.*, 2017; Sun *et al.*, 2017; Wilson *et al.*, 2019). The present study provides *in vivo* mechanistic evidence suggesting that metastatic spread of endometriotic tissue to the ovaries, omentum and peritoneum occurs as a result of invasive endometrial phenotypes. ARID1A and PIK3CA are commonly mutated in the endometrium, and mutation of the endometrium can result in a number of invasive phenotypes, including endometriosis, adenomyosis, endometrial cancer and ovarian cancer. Adenomyosis is the result of direct invasion into the myometrium, while endometriosis forms following invasion distally into the peritoneum or ovary. The collective migration of mutant endometrial cells undergoing partial EMT may enhance the invasive properties of ectopic endometriotic tissue, permitting invasion of the surrounding tissue.

The model presented herein mimics the natural spread of endometriotic tissue via retrograde translocation. While mice do not menstruate, our data support the idea that anatomic barriers obstructing the retrograde spread of invasive endometrial tissue prevent the disease. In our mouse model, removal of the oviducts and

bursal membrane promoted the spread of invasive endometrial cells harboring ARID1A and PIK3CA mutations from the ipsilateral uterine horn. Established mouse models of endometriosis have been limited by the requirement of tissue transplantation, steroid hormone treatment or genetic perturbation in tissues other than the endometrial epithelium (King *et al.*, 2016). The present model recapitulates the retrograde traversal of tissue, while mimicking the heterogeneous phenotypes presented in endometriosis patients. This model may provide utility in studying the mechanisms by which endometriosis spreads to particular tissues. However, the present model has its own limits. Due to uterine endometrial dysfunction and subsequent vaginal bleeding (Wilson *et al.*, 2019), *LtfCre<sup>0/+</sup>; (Gt)R26Pik3ca<sup>\*H1047R</sup>; Arid1a<sup>fl/fl</sup>* mice have a short lifespan, and disease progression cannot be tracked in the long term. Furthermore, *LtfCre<sup>0/+</sup>; (Gt)R26Pik3ca<sup>\*H1047R</sup>; Arid1a<sup>fl/fl</sup>* display a phenotype which is 100% penetrant throughout the endometrium and, as such, all endometrial epithelia harbor ARID1A and PIK3CA mutations, which is not the case in patients with endometriosis. Even still, many endometriotic lesions harbor mutations other than ARID1A or PIK3CA, suggesting that other genetic mutations may suffice for the invasive phenotypes observed in endometriosis.

Given the widespread acceptance of the implantation theory, it has been suggested that an inappropriate differentiation of the



and R.L.C.; funding acquisition, M.R.W. and R.L.C.; supervision, R.L.C.

## Funding

American Cancer Society Postdoctoral Fellowship (PF-17-163-02-DDC to M.R.W.); Innovative Translational Grant from the Mary Kay Foundation (026-16 to R.L.C.); Liz Tilberis Early Career Award from the Ovarian Cancer Research Fund Alliance (OCRFA) (457446 to R.L.C.).

## Conflict of interest

The authors declare no competing interests.

## References

- Adams JR, Xu K, Liu JC, Agamez NM, Loch AJ, Wong RG, Wang W, Wright KL, Lane TF, Zacksenhaus E *et al.* Cooperation between *Pik3ca* and *p53* mutations in mouse mammary tumor formation. *Cancer Res* 2011;**71**:2706–2717.
- Alimi Y, Iwanaga J, Loukas M, Tubbs RS. The clinical anatomy of endometriosis: a review. *Cureus* 2018;**10**:e3361.
- Anglesio MS, Papadopoulos N, Ayhan A, Nazeran TM, Noe M, Horlings HM, Lum A, Jones S, Senz J, Seckin T *et al.* Cancer-associated mutations in endometriosis without cancer. *N Engl J Med* 2017;**376**:1835–1848.
- Aoki D, Katsuki Y, Shimizu A, Kakinuma C, Nozawa S. Successful heterotransplantation of human endometrium in SCID mice. *Obstet Gynecol* 1994;**83**:220–228.
- Bartley J, Julicher A, Hotz B, Mechsner S, Hotz H. Epithelial to mesenchymal transition (EMT) seems to be regulated differently in endometriosis and the endometrium. *Arch Gynecol Obstet* 2014;**289**:871–881.
- Berg A, Hoivik EA, Mjos S, Holst F, Werner HM, Tangen IL, Taylor-Weiner A, Gibson WJ, Kusunmano K, Wik E *et al.* Molecular profiling of endometrial carcinoma precursor, primary and metastatic lesions suggests different targets for treatment in obese compared to non-obese patients. *Oncotarget* 2015;**6**:1327–1339.
- Bergqvist A, Jeppsson S, Kullander S, Ljungberg O. Human uterine endometrium and endometriotic tissue transplanted into nude mice. Morphologic effects of various steroid hormones. *Am J Pathol* 1985;**121**:337–341.
- Budiu RA, Diaconu I, Chrissluis R, Dricu A, Edwards RP, Vlad AM. A conditional mouse model for human MUC1-positive endometriosis shows the presence of anti-MUC1 antibodies and Foxp3+ regulatory T cells. *Dis Model Mech* 2009;**2**:593–603.
- Burney RO, Giudice LC. Pathogenesis and pathophysiology of endometriosis. *Fertil Steril* 2012;**98**:511–519.
- Chandler RL, Brennan J, Schisler JC, Serber D, Patterson C, Magnuson T. ARID1a-DNA interactions are required for promoter occupancy by SWI/SNF. *Mol Cell Biol* 2013;**33**:265–280.
- Chandler RL, Damrauer JS, Raab JR, Schisler JC, Wilkerson MD, Didion JP, Starmer J, Serber D, Yee D, Xiong J *et al.* Coexistent ARID1A-PIK3CA mutations promote ovarian clear-cell tumorigenesis through pro-tumorigenic inflammatory cytokine signalling. *Nat Commun* 2015;**6**:6118.
- Cheng CW, Licence D, Cook E, Luo F, Arends MJ, Smith SK, Print CG, Charnock-Jones DS. Activation of mutated K-ras in donor endometrial epithelium and stroma promotes lesion growth in an intact immunocompetent murine model of endometriosis. *J Pathol* 2011;**224**:261–269.
- Chui MH, Wang TL, Shih IM. Endometriosis: benign, malignant, or something in between? *Oncotarget* 2017;**8**:78263–78264.
- Cummings AM, Metcalf JL. Induction of endometriosis in mice: a new model sensitive to estrogen. *Reprod Toxicol* 1995;**9**:233–238.
- Daikoku T, Ogawa Y, Terakawa J, Ogawa A, DeFalco T, Dey SK. Lactoferrin-iCre: a new mouse line to study uterine epithelial gene function. *Endocrinology* 2014;**155**:2718–2724.
- Dinulescu DM, Ince TA, Quade BJ, Shafer SA, Crowley D, Jacks T. Role of K-ras and Pten in the development of mouse models of endometriosis and endometrioid ovarian cancer. *Nat Med* 2005;**11**:63–70.
- Giudice LC, Kao LC. Endometriosis. *Lancet* 2004;**364**:1789–1799.
- Greaves E, Cousins FL, Murray A, Esnal-Zufiaurre A, Fassbender A, Horne AW, Saunders PT. A novel mouse model of endometriosis mimics human phenotype and reveals insights into the inflammatory contribution of shed endometrium. *Am J Pathol* 2014;**184**:1930–1939.
- Grummer R, Schwarzer F, Balczyk K, Hess-Stumpp H, Regidor PA, Schindler AE, Winterhager E. Peritoneal endometriosis: validation of an in-vivo model. *Hum Reprod* 2001;**16**:1736–1743.
- Halme J, Hammond MG, Hulka JF, Raj SG, Talbert LM. Retrograde menstruation in healthy women and in patients with endometriosis. *Obstet Gynecol* 1984;**64**:151–154.
- Hastings JM, Jackson KS, Mavrogianis PA, Fazleabas AT. The estrogen early response gene FOS is altered in a baboon model of endometriosis. *Biol Reprod* 2006;**75**:176–182.
- Hirata T, Osuga Y, Yoshino O, Hirota Y, Harada M, Takemura Y, Morimoto C, Koga K, Yano T, Tsutsumi O *et al.* Development of an experimental model of endometriosis using mice that ubiquitously express green fluorescent protein. *Hum Reprod* 2005;**20**:2092–2096.
- Kelso TWR, Porter DK, Amaral ML, Shokhirev MN, Benner C, Hargreaves DC. Chromatin accessibility underlies synthetic lethality of SWI/SNF subunits in ARID1A-mutant cancers. *Elife* 2017;**6**.
- Kim TH, Yoo JY, Wang Z, Lydon JP, Khatri S, Hawkins SM, Leach RE, Fazleabas AT, Young SL, Lessey BA *et al.* ARID1A is essential for endometrial function during early pregnancy. *PLoS Genet* 2015;**11**:e1005537.
- King CM, Barbara C, Prentice A, Brenton JD, Charnock-Jones DS. Models of endometriosis and their utility in studying progression to ovarian clear cell carcinoma. *J Pathol* 2016;**238**:185–196.
- Lac V, Nazeran TM, Tessier-Cloutier B, Aguirre-Hernandez R, Albert A, Lum A, Khattra J, Praetorius T, Mason M, Chiu D *et al.* Oncogenic mutations in histologically normal endometrium: the new normal? *J Pathol* 2019.
- Lakshminarasimhan R, Andreu-Vieyra C, Lawrenson K, Duymich CE, Gayther SA, Liang G, Jones PA. Down-regulation of ARID1A is sufficient to initiate neoplastic transformation along with epigenetic reprogramming in non-tumorigenic endometriotic cells. *Cancer Lett* 2017;**401**:11–19.

- Li C, Xu ZL, Zhao Z, An Q, Wang L, Yu Y, Piao DX. ARID1A gene knockdown promotes neuroblastoma migration and invasion. *Neoplasma* 2017;**64**:367–376.
- Matsuzaki S, Darcha C. Epithelial to mesenchymal transition-like and mesenchymal to epithelial transition-like processes might be involved in the pathogenesis of pelvic endometriosis. *Hum Reprod* 2012;**27**:712–721.
- Mogensen JB, Kjaer SK, Mellekjær L, Jensen A. Endometriosis and risks for ovarian, endometrial and breast cancers: a nationwide cohort study. *Gynecol Oncol* 2016;**143**:87–92.
- Muzumdar MD, Tasic B, Miyamichi K, Li L, Luo L. A global double-fluorescent Cre reporter mouse. *Genesis* 2007;**45**:593–605.
- Poole EM, Lin WT, Kvaskoff M, De Vivo I, Terry KL, Missmer SA. Endometriosis and risk of ovarian and endometrial cancers in a large prospective cohort of U.S. nurses. *Cancer Causes Control* 2017;**28**:437–445.
- Rendi MH, Muehlenbachs A, Garcia RL, Boyd KL. Female Reproductive System. In: *Comparative Anatomy and Histology*. Elsevier, 2012,253–284
- Rossi G, Somigliana E, Moschetta M, Santorsola R, Cozzolino S, Filardo P, Salmaso A, Zingrillo B. Dynamic aspects of endometriosis in a mouse model through analysis of implantation and progression. *Arch Gynecol Obstet* 2000;**263**:102–107.
- Samartzis EP, Samartzis N, Noske A, Fedier A, Caduff R, Dedes KJ, Fink D, Imesch P. Loss of ARID1A/BAF250a-expression in endometriosis: a biomarker for risk of carcinogenic transformation? *Mod Pathol* 2012;**25**:885–892.
- Sampson JA. Peritoneal endometriosis due to the menstrual dissemination of endometrial tissue into the peritoneal cavity. *Am J Obstet Gynecol* 1927;**14**:422–469.
- Suda K, Nakaoka H, Yoshihara K, Ishiguro T, Tamura R, Mori Y, Yamawaki K, Adachi S, Takahashi T, Kase H et al. Clonal expansion and diversification of cancer-associated mutations in endometriosis and normal endometrium. *Cell Rep* 2018;**24**:1777–1789.
- Sun X, Wang SC, Wei Y, Luo X, Jia Y, Li L, Gopal P, Zhu M, Nassour I, Chuang JC et al. Arid1a has context-dependent oncogenic and tumor suppressor functions in liver cancer. *Cancer Cell* 2017;**32**:574–589 e576.
- Vierbuchen T, Ling E, Cowley CJ, Couch CH, Wang X, Harmin DA, Roberts CWM, Greenberg ME. AP-1 transcription factors and the BAF complex mediate signal-dependent enhancer selection. *Mol Cell* 2017;**68**:1067–1082 e1012.
- Wiegand KC, Lee AF, Al-Agha OM, Chow C, Kalloger SE, Scott DW, Steidl C, Wiseman SM, Gascoyne RD, Gilks B et al. Loss of BAF250a (ARID1A) is frequent in high-grade endometrial carcinomas. *J Pathol* 2011;**224**:328–333.
- Wilson MR, Reske JJ, Holladay J, Wilber GE, Rhodes M, Koeman J, Adams M, Johnson B, Su RW, Joshi NR et al. ARID1A and PI3-kinase pathway mutations in the endometrium drive epithelial transdifferentiation and collective invasion. *Nat Commun* 2019;**10**.
- Yan HB, Wang XF, Zhang Q, Tang ZQ, Jiang YH, Fan HZ, Sun YH, Yang PY, Liu F. Reduced expression of the chromatin remodeling gene ARID1A enhances gastric cancer cell migration and invasion via downregulation of E-cadherin transcription. *Carcinogenesis* 2014;**35**:867–876.
- Zamah NM, Dodson MG, Stephens LC, Buttram VCJ, Besch PK, Kaufman RH. Transplantation of normal and ectopic human endometrial tissue into athymic nude mice. *Am J Obstet Gynecol* 1984;**149**:591–597.